DOI: 10.15480/882.9342

Eighth International Symposium on Marine Propulsors
smp'24, Berlin, Germany, March 2024

Propeller Load Variations for Maneuvering Ships in Waves

Joost Moulijn[1], Roberto Tonelli[1] and Udai Shipurkar[1]

[1]Maritime Research Institute Netherlands (MARIN), Wageningen, The Netherlands

ABSTRACT

This paper presents a method that can predict the load variations on propellers of ships that are maneuvering in waves. A *two time-scales* approach is followed.

The method consist of a calm water maneuvering time simulation method and a frequency domain seakeeping method. The mean and low frequent wave drift forces are applied as an external force in the maneuvering simulations. The wave frequent motions and propeller inflow variations are superimposed on the simulation result. These inflow variations are used to predict the propeller thrust and torque variations.

The results are compared with model experiments for the DTMB 5415M combatant. The experiments and simulations are in reasonably good agreement. The simulation method can capture several relevant phenomena that are observed in the model experiments.

Keywords

Propulsion in waves, Propulsion during maneuvering, Time simulation, Digital twin.

1 INTRODUCTION

The energy transition requires major innovations of the propulsion system on board of ships. The engine rooms of the future will contain many new systems such as fuel cells, battery packs, super capacitors and internal combustion engines that are running on alternative fuels. The design, verification and validation of these novel Propulsion Power and Energy (PPE) systems require accurate simulation models for the dynamic power demand by the propeller. Studies have shown that effects of propeller load variations range from increased fuel consumption and emissions (Tavakoli et al 2020, Yum et al 2017) to reducing efficiencies and power quality in the connected electrical systems (Hou et al 2017, Nasiri et al 2021). This is further exacerbated when fuels and energy conversion technologies with lower dynamic response capabilities are used, such as fuel cells and combustion engines running on alternate fuels. Furthermore, the operating limits of these components effects the available torque for the propeller, and thereby affecting ship motions.

This paper presents a simulation model that can predict load variations on the PPE system for ships that are maneuvering in waves. A two-time scale approach is followed where the maneuvering motions and the motions due to low frequent wave drift forces are solved by a time domain simulation method. The wave frequent motions and propeller inflow variations are superimposed on result of the time simulation method.

For a ship that is sailing in waves, the wave forces (and moments) can be split in two components: first order (wave frequent) forces and second order drift forces. The first order forces have a zero mean value, the variations happen at frequencies that are equal to the ship-wave encounter frequencies, and the magnitude is proportional to the height of the waves. The second order forces, also called drift forces, are proportional to the wave height squared (at least up to moderate wave heights, hence second order). The drift forces have a non-zero mean value and, when the ship sails in irregular waves, they are varying at a much lower frequency than the wave frequency. These low frequent variations are related to the occurrence of wave groups. Sometime the ship is encountering several high waves. This results in large drift forces. A few minutes later the sea is more quiet and the drift forces are low. The mean value of the drift forces in sailing direction is often called *added resistance due to waves*.

The basis of the present simulation model is a calm water maneuvering time simulation model. An additional force is introduced that represents the (mean and low frequent) drift forces. This force causes low frequent ship speed variations and consequent propeller inflow variations. The wave frequent ship motions and propeller inflow variations are calculated by means of a 3D linear frequency domain seakeeping code. This method calculates the disturbed wave pattern around the ship, which appears to be crucial for an accurate prediction of the propeller inflow variations. The wave frequent

motions and inflow variations are simply superimposed on the low frequent motions and inflow that are predicted by the time simulation method. The seakeeping method also predicts the drift forces.

Section 2 describes the various elements of the simulation method. Special attention is payed to the models for propeller inflow, both for the maneuvering model and the seakeeping model.

Section 3 presents a comparison of simulation and model test results for the DTMB 5415M combatant. These experiments include calm water maneuvering experiments (turning circles and zig-zag maneuvers) as well as maneuvering in waves experiments (heading and track keeping) in regular and irregular waves and for various headings and ship speeds.

Section 4 presents some results where the interaction with the engine is taken into account. The control settings for the propeller revolutions appear to have an important effect on the load variations that the PPE system experiences.

2 DESCRIPTION OF THE SIMULATION MODEL

A ship that is sailing in waves is subject to a large variety of forces, such as gravitational forces, hydrostatic forces, wind forces, propulsion forces, steering forces, maneuvering reaction forces of the hull (including resistance) and forces due to the ocean waves. The ship's motions are solved in the time domain using MARIN's eXtensible Modeling Framework (XMF) (Abbing 2015). This framework contains models for all different force components. All forces acting on the hull body (or multiple bodies) are summed and the equations of motion (of each body) are solved.

The approach used in this paper is the *two time-scales* approach, introduced by Yasukawa & Nakayama (2009). The approach solves the low and high frequent motions separately from each other: the low frequent motions are driven by the maneuvering and the second order wave drift forces, including control devices such as propellers and rudders. The high frequent motions are the traditional seakeeping surge, sway, heave, roll, pitch and yaw (RAOs) motions. The sum of the low frequency and the high frequency motions is the final motion of the ship.

The approach computes and uses the time-varying second order wave drift forces because the full Quadratic Transfer Function (QTF) is used. Furthermore, the mean and slowly varying wave forces are speed dependent. By using directly the frequency domain wave drift forces, the approach ensures that the wave excitation is as good as the (linear) frequency domain one.

This approach is also described by Quadvlieg & Rapuc (2019), including a validation against model tests and a benchmark time domain tool (FREDYN) for the 5415M navy vessel.

The following subsections describe the used coordinate system, the maneuvering model and the seakeeping model, where there is particular focus on the water inflow to the propeller disk. A fourth subsection describes the coupling between the maneuvering in waves model and the engine room model.

2.1 Coordinate system

Several coordinate systems are used in the various components of the simulation model. There is a global coordinate stem that is used to track the position of the ship and to define the ocean waves. There is a ship fixed coordinate system with its origin at the ship's center of gravity (SOG), x-axis towards the bow, y-axis towards port and z-axis in upwards direction. And there is a *yawed* coordinate system that also has its origin at the COG of the ship, but with respect to the global system it is only rotated about the z-axis. Furthermore, there are local coordinate systems at the propeller and rudder.

A complete description of all coordinate system goes beyond the scope of this paper. However, the most important definitions are show in Figure 1. The figure shows the x, y and z-axis of the yawed coordinate system, the ship velocity vector V with its components u and v in x-and y direction as well as the rotation velocity r about the z-axis. The ship is sailing under a drift angle β. A positive rudder angle δ is indicated as well as the incoming wave direction μ.

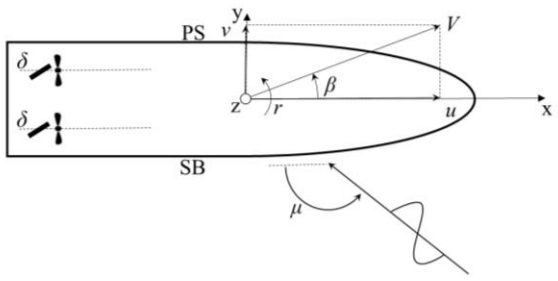

Figure 1: Coordinate system

2.2 Maneuvering Model

The calm water maneuvering model consists of a hydrostatic model, a coefficient model for the hydrodynamic forces on the hull, a rudder model and a propeller model. They are briefly described. Subsequently, the model for the flow into the propeller disk is elaborated.

2.2.1 Hydrostatics

The static equilibrium is dominated by the balance between weight and buoyancy. Due to the quasi-static motion, the balance can be disturbed by a shift of the position of the center of gravity, a shift of the position of center of buoyancy, and a change in the magnitude of the buoyancy. The linear hydrostatics model these effects and the influence on the ship stability, by determining a linearized stiffness matrix at the center of gravity (from a linear restoring matrix at the center of floatation and a spring matrix at the center of gravity).

2.2.2 Hull forces model

The maneuvering reaction forces are modelled via coefficients multiplied by the motion derivatives (ship

velocities) in surge, sway, roll and yaw and the heel angle (Ferrari et al 2022). The added mass and inertia are modelled via coefficients multiplied by the ship accelerations. These coefficients fit captive maneuvering model test results.

2.2.3 Rudder model

The rudder mathematical model (Ferrari et al 2022), provides the rudder reaction forces and moments. This model describes the flow around the rudder in maneuvering conditions, averaging speed and force components in a single point of application, and with simple, robust, and widely applicable formulas. The model is defined by the dimensions, location, and inclination angle in the y-z plane. The model includes also the effect of an accelerated inflow when the rudder is positioned in a propeller slip stream. Moreover, the model includes the effect of a straightened inflow due to the presence of the hull. The rudder does not react to the individual wave velocity but only to the ship speed and local drift angle variations.

2.2.4 Propeller model

The propeller model is based on four quadrant open water characteristics (Kuiper 1992). Figure 2 shows an example of four quadrant open water curves. In order to avoid confusion, the torque coefficient C_Q is plot with a minus sign.

The propeller thrust and torque are made non dimensional in a different form than the common J - K_T - K_Q curves:

$$
\begin{aligned}
C_T(\beta) &= \frac{T}{\frac{1}{2}\cdot\rho\cdot V_R^2\cdot\frac{\pi}{4}\cdot D^2} \\
C_Q(\beta) &= \frac{Q}{\frac{1}{2}\cdot\rho\cdot V_R^2\cdot\frac{\pi}{4}\cdot D^3} \\
V_R &= \sqrt{V_a^2+(0.7\cdot\pi\cdot n\cdot D)^2} \\
\beta &= \tan^{-1}\left(\frac{V_a}{0.7\cdot\pi\cdot n\cdot D}\right)
\end{aligned}
\qquad (1)
$$

where T is thrust, Q is torque, ρ is water density, D is the propeller diameter, n is the propeller rotation rate and V_a is the propeller advance velocity.

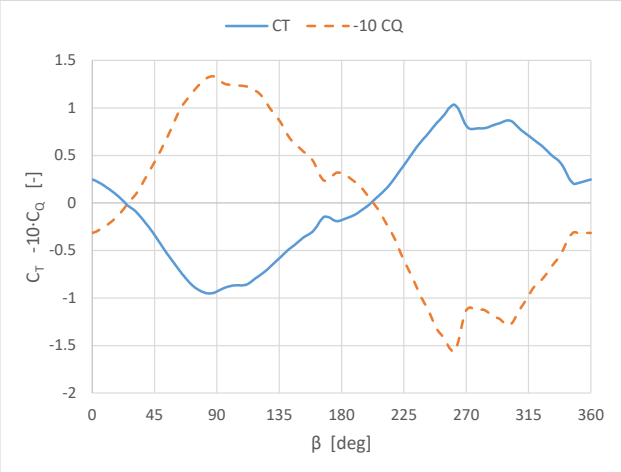

Figure 2: Four quadrant open water characteristics

The advantage of using four quadrant open water characteristics over regular open water characteristics is that they always provide results, also for uncommon conditions like non-rotating (blocked) propellers, or negative advance speed and positive rotation rate. During maneuvering simulations one never knows upfront what conditions will be encountered. The model is robust and the computational effort is small.

A disadvantage of the model is that it only predicts the axial forces on the propeller (i.e. thrust and torque). It does not predict any transverse force components. However, when transverse propeller forces are compared with rudder forces, it appears that they are an order of magnitude smaller. This conclusion is based on RANS calculations for the ONR Tumblehome combatant sailing under prescribed drift and rotation with a wide range of rudder angles.

2.2.5 Propeller Inflow Model

In the CRS[1] SALSA[2] working group an extensive set of CFD computations was done. The main goal of this CFD campaign was to improve the predictions of propeller thrust and torque and rudder forces for ships sailing in harsh weather and thus at low speed. The inflow velocity field to the propellers (and rudders) was calculated for two single screw ships, a coaster and a container vessel, and three twin screw ships, a cruise vessel and two naval combatants. The ships were sailing at a constant speed (in calm water) under pure drift, pure rotation or a combination of drift and rotation as illustrated in Figure 3.

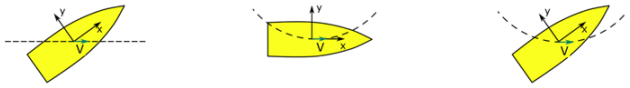

Figure 3: Ship sailing under pure drift (left), pure rotation (middle) and combination (right)

A wide range of drift angles and rates of turn was investigated. Furthermore, the effects of ship speed and propeller loading on the (effective) wake field were investigated. However, these appeared to be relatively small.

Figure 4 shows an example of the inflow to the starboard propeller of the ONRT combatant sailing under a pure drift angle of 25°. For this positive drift angle, the starboard propeller is in the wake of the ship, while the port propeller is more in free stream.

Figure 4 clearly shows the presence of a strong vortex that is flowing into the propeller disk. The vortex originates from the port bilge keel. It is advected under the ship, where it may be amplified by the presence of the skeg. Subsequently, the vortex flows right through the starboard propeller disk. This is clearly shown in Figure 5.

[1] Cooperative Research Ships: A consortium of yards, navies, classification societies, suppliers to maritime industry and research institutes, initialized by MARIN.

[2] Safety At Low Speed Assessment

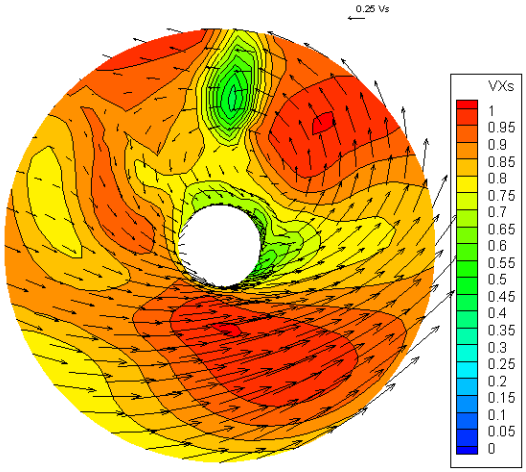

Figure 4: Effective wake field for the starboard propeller of the ONRT combatant sailing under 25° of pure drift.

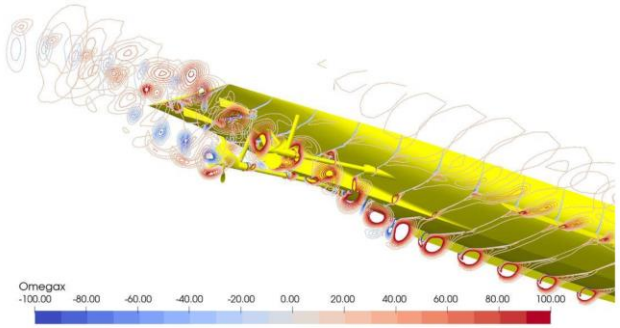

Figure 5: Vortex flowing through the starboard propeller of the ONRT combatant

This vortex has a major impact on the propeller thrust and torque. It is co-rotating with the propeller (the propellers of ONRT are rotating inward over the top). This results in a strong reduction of the effective rotation rate of the propeller.

In order to apply the calculated wake fields in a useful way in the maneuvering simulation method, the velocities are averaged over the propeller disk as follows:

$$\bar{v} = \frac{1}{A}\iint_A v \cdot dA \qquad (2)$$

where A is the propeller disk area and v is one of the following velocity components: the axial velocity v_x, the horizontal transverse component v_y, the vertical transverse component v_z or the tangential velocity component divided by the radius v_t/r. The average of the later component represents an effective solid body rotation of the inflow to the propeller. This can be applied as a correction to the propeller rotation rate. From now on this will be referred to as *inflow swirl*.

In order to show the validity and usefulness of this approach, the averaged values of the various wake components are used to construct averaged wake fields. These wake fields are subsequently used in PROCAL[3] calculations and the resulting propeller forces are compared.

Figure 6 shows the averaged wakes based on the wake field that is shown in Figure 4. The top left wake is based on the averaged axial inflow only. The top right wake is based on the axial and the horizontal and vertical transverse inflow components. The bottom left wake is based on the axial and the swirl inflow components. Finally, the bottom right wake is based on all averaged inflow components. The color scale is identical to that of Figure 4, but as the axial inflow is constant (0.861 times ship speed) it only shows a single color.

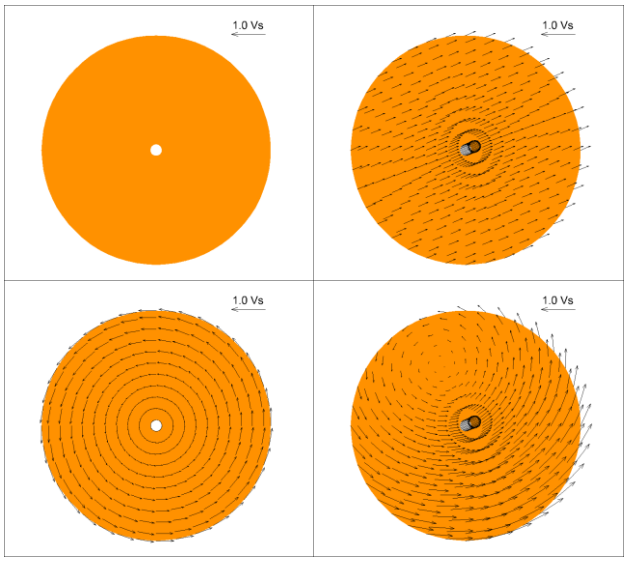

Figure 6: Wake fields constructed from averaged values: axial only (top left), axial and transverse (top right), axial and swirl (bottom left), and axial and transverse and swirl (bottom right)

Such wake fields were generated for drift angles from 0° to 30°. Subsequently, the propeller forces were calculated by means of PROCAL. Figure 7 presents the results. The top chart shows the axial force, the middle chart shows the horizontal transverse force and the bottom chart shows the vertical transverse force. Each chart shows results of the following calculations: RANS-BEM (Rijpkema et al 2013) coupled calculations (diamond markers), RANS-RANS sliding interface calculations (+ markers, only 0° and 25° drift), and then PROCAL calculations for the full effective wake (as in Figure 4, black line in Figure 7), for the axial only wake (as in Figure 5 top left, red line), for the axial plus transverse wake (Figure 5 top right, blue line), for the axial plus swirl wake (Figure 5 bottom left, purple line) and for the axial plus transverse plus swirl wake (Figure 5 bottom right, green line). Furthermore, the axial force chart (top) also shows results using open water characteristics including an RPM correction for swirl (dashed purple line with markers).

[3] MARIN's BEM based propeller analysis code (Vaz 2005, Vaz & Bosschers 2006)

It must be noted that the PROCAL calculations were done for a very low speed: a ship speed of 4 knots and a propeller rotation rate of 17.43 RPM. As a consequence, the buoyancy of the blades is a relatively large contribution to the propeller forces. This is the reason for the large forces in z-direction (bottom chart of Figure 7). In the axial only and axial and swirl result, the transverse hydrodynamic forces are zero. The constant z-forces of 11.7 [kN] is entirely due to buoyancy.

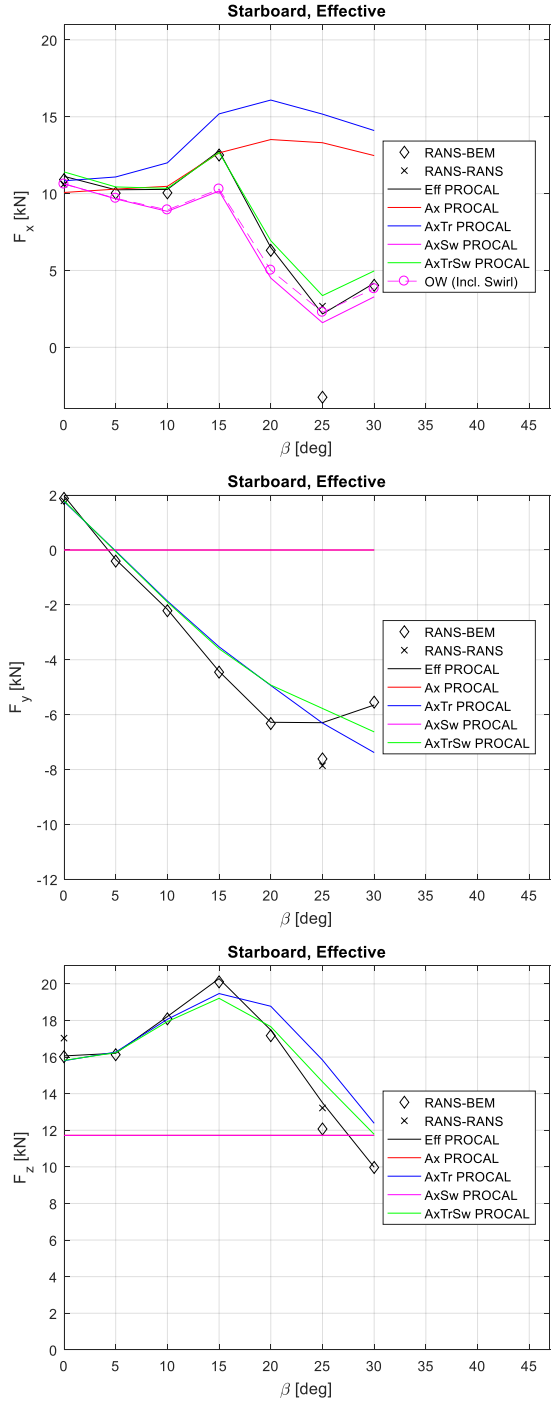

Figure 7: Comparison of propeller forces as function of drift angle β: axial (top), horizontal (middle) and vertical (bottom)

There is one RANS-BEM result (at β = 25°) not in line with the other results. This is caused by a poor convergence of the BEM (i.e. PROCAL) results in the coupled RANS-BEM procedure. In the later PROCAL calculations, the convergence was improved through the application of a different mesh.

One striking result is the almost zero thrust (axial force) for the 25° drift condition. This is caused by the strong vortex (i.e. swirl) that is present in the wake field. It is co-rotating with the propeller, which results in a strong reduction of the effective propeller rotation rate. If the rotational direction of the propeller would be opposite, the effect on thrust (and torque) would also be opposite.

The results in Figure 7 clearly show that including the swirl is very important in order to obtain a good prediction of the propeller thrust. The same applies to the propeller torque. The effect of the transverse inflow velocities is much more limited. For the transverse forces, it appears that the swirl has little effect, but now the transverse inflow velocity is of crucial importance.

The thrust and torque prediction (torque not shown), based on the open water characteristics with an RPM correction for swirl, follows the PROCAL calculations quite well. The transverse propeller forces are considered less important for the maneuvering behavior of the ship. Moreover, the main goal of the present work is an adequate prediction of the propeller torque. Therefore, the propeller model for the maneuvering time simulation method is based on open water characteristics with a swirl correction.

There is one other compromise in the maneuvering simulation method regarding the propeller inflow model. The averaged axial and swirl inflow velocity depend on the drift and on the rate of turn of the ship. However, the CFD calculations do not cover a full matrix of these parameters. Therefore, they are combined into a local crossflow angle at the propellers as is shown in Figure 8. When the averaged inflows for pure drift, pure rotation and combined drift and rotation are plot as function of the local crossflow angle, this simplification appears to be not entirely justifiable. Nevertheless, because of a lack of data, this simplification is maintained for now.

2.3 Seakeeping Model

The seakeeping code SEACAL is used to predict the wave frequent ship motions and the drift forces. SEACAL is a 3 dimensional panel method that is similar to methods by Nakos (1990), Bertram (1990), Van ‘t Veer (1989) and Bunnik (1998). This method can accurately predict the disturbed waves around the ship, unlike a strip theory method that only consider radiated and diffracted waves in transverse direction.

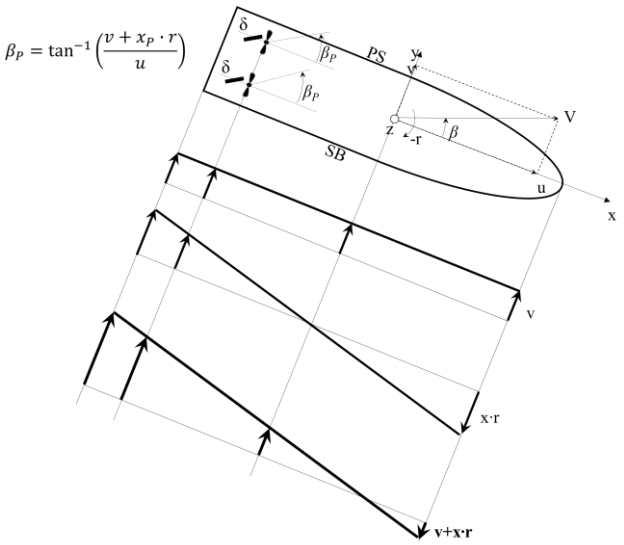

Figure 8: Combining drift and rotation into a local crossflow

SEACAL is a panel method that is based on potential flow. It is a linear method, and therefore, in theory, only valid for low waves. Nevertheless, linear seakeeping methods still can produce very useful results for higher waves, at least for displacement ships. Linearity also opens the possibility to solve the problem in the frequency domain. This implies that SEACAL only considers regular (i.e. sinusoidal) waves. Results for irregular waves can be obtained by superposition of results for regular waves with a range of frequencies.

SEACAL has two modelling options for the free surface. In the first option, the forward speed effects in the boundary condition on the free surface are neglected. This has the advantage that no panels are required on the free surface, which results in a much smaller computational problem. Popularly said, the hull is then covered with panels with a distribution of special sources that already fulfil the free surface boundary condition. This method will be referred to as *zero speed Green function*.

In the second option the (linearized) free surface boundary condition including forward speed effects is applied. This also requires panels on the free surface in a sufficiently large area around the hull. A wave damping zone is applied at some distance from the hull to prevent wave reflections from the edges of the free surface panel mesh. This results in a much larger matrix that must be solved, but the wave pattern around the ship is much more realistic. This modelling option is called *Rankine* method.

2.3.1 Propeller inflow variations

In order to predict the inflow variations due to waves and motions of the ship, a number of reference points is placed at the location of the two propeller disks. In the present study point were located at the propeller center, and at 0.2R, 0.6R and 1.0R (R is the propeller radius) and at angular positions of 0, 45, …, 315 deg. Figure 9 shows a panel mesh on the hull and the reference points at the propellers for the DTMB 5415M combatant. This ship is used as validation case in Section 3.

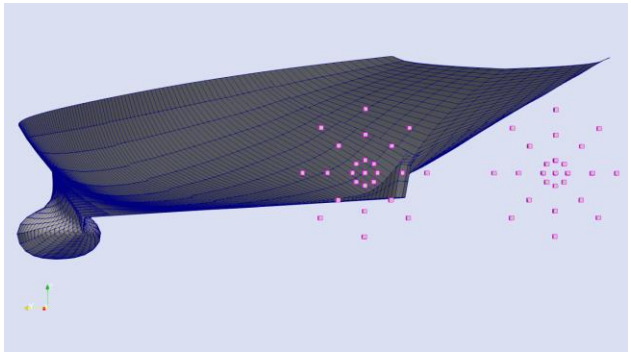

Figure 9: Hull mesh and reference points at the propellers for the DTMB 5415M combatant

At these reference points, the relative velocity of the water with respect to the (ship fixed) reference point is calculated. It follows from subtracting the absolute velocity of a reference point from the absolute water velocities at that reference point. This relative velocity is the inflow variation to the propeller in the subject reference point. This variation is superimposed on the low frequent inflow variations that follow from the maneuvering time simulation method.

Figure 10 shows the Response Amplitude Operator (RAO) for the axial component of the velocity at the propeller center. The figure plots the amplitude of the velocity variations dived by the wave amplitude as function of the wave frequency. It shows results for a ship speed of 12 knots and a heading of 135° with respect to the waves (bow quartering waves, on starboard). The figure shows results for the port (PS) and the starboard (SB) propeller. Furthermore, it shows results that are based on the motions of the ship and the orbital velocities of the undisturbed waves only, as well as results that also include the effect of the disturbance of the incoming waves, i.e. the diffracted waves, and the radiated waves due to the motions of the ship. Figure 10 clearly shows the importance of including the effects of the radiated and diffracted waves. In particular on the port side, which is the leeward side, there is a huge reduction of the inflow variation due to the radiated and diffracted waves, because of the shielding effect of the hull. The effect on the SB, i.e. windward, side is also significant, but not as strong as for the leeward side.

Figure 11 Shows similar RAOs for the axial propeller inflow at the propeller center. This figure compares results that were obtained with the zero speed Green function (ZSGF) and the Rankine methods. The figure clearly shows that the ZSGF method does not fully capture the shielding effect of the hull towards the leeward (PS) propeller. In most cases, the ZSGF method can predict the ship motions quite accurately (when the ship speed is not too high). For the velocity variations at the propeller this is not the case. A realistic free surface modeling is also important for the water velocities around the ship.

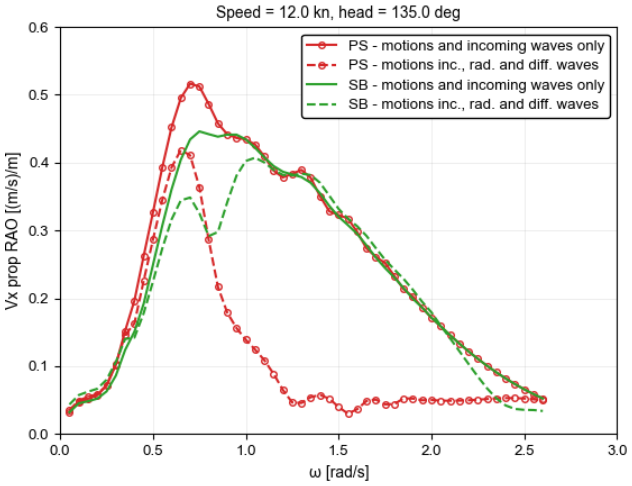

Figure 10: Effect of radiated and diffracted waves on the RAO for the axial propeller inflow velocity at the propeller center

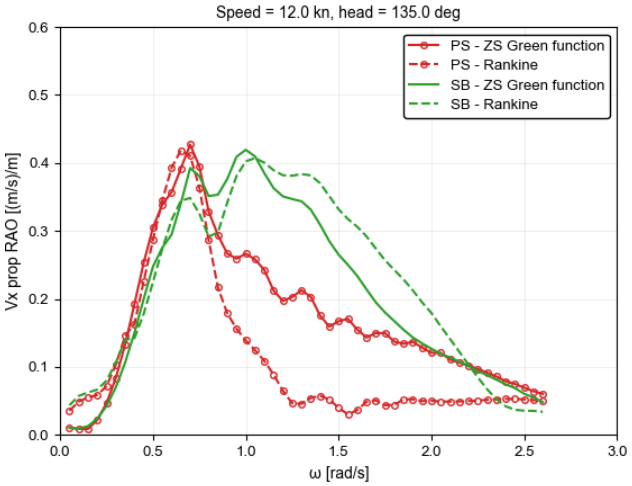

Figure 11: Effect of free surface method on the RAO for the axial propeller inflow velocity at the propeller center

Figure 12 also shows RAOs for the axial component of the velocity at the propeller (including radiated and diffracted waves). This figure shows results for different reference points in the starboard propeller disk: again the propeller center and also for points at the propeller tip radius (1.0R) at angular positions of 0°, 90°, 180° and 270°, where 0° is the bottom position, 90° is on the inner (port) side of the SB propeller disk, 180° is the top position and 270° is on the outside. Figure 12 clearly shows that there is significant variation over the propeller disk. The strongest variations occur on the top and on the outside of the propeller.

Similar phenomena can be observed for the horizontal and vertical transverse velocities in the propeller disk. These transverse velocity components have a limited effect on the propeller thrust and torque, but they are of crucial importance when the cavitation behavior of the propellers is considered. The main focus of the present paper is on propeller thrust and torque, and therefore on the axial velocity variations.

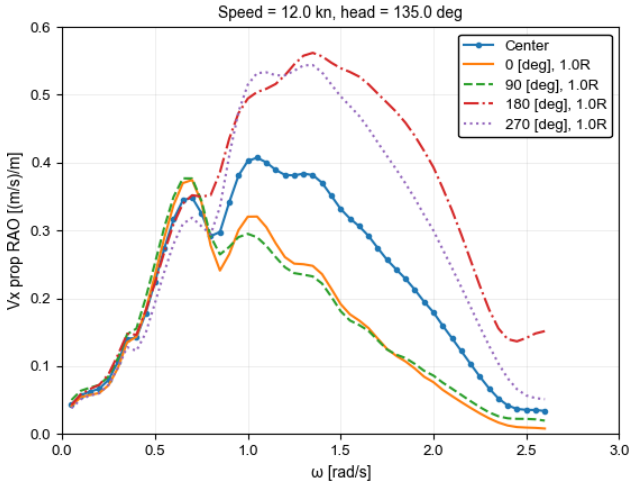

Figure 12: RAO for the axial propeller inflow velocity at various points on the starboard propeller disk

The axial velocities in the reference points at the propeller disk are averaged (weighted with the propeller radius). This averaged axial velocity is used in the propeller model that was described in Section 2.2.4 of this paper.

2.4 Coupling with Engine Simulations

MARIN is developing the Zero Emission Laboratory (ZEL), a unique facility where the engine room of the future can be tested at a reduced scale. The present simulation model will be coupled to the ZEL and its digital twin, the v-ZEL, in the form of a co-simulation. This implies 2-ways interaction. When the engine or electric motor cannot maintain the propeller RPM due to the load variations, this also has an effect on the maneuvering behavior of the ship, which, on its turn, has an effect on the propeller load variations.

The boundary between the hydrodynamic ship simulation and the engine room simulation is chosen on the propeller blade surface. This implies that the hydrodynamic propeller torque is sent from the maneuvering in waves simulation to the simulation of the propulsion power and energy (PPE) system. The shaft rotation is solved in the PPE simulation. Subsequently, the resulting propeller rotation rate is send back to the maneuvering in waves simulation.

For the PPE simulations it is important to include the wave frequent torque variations. The introduction of the wave frequent inflow variations, however, also implies the introduction of wave frequent thrust variations in the otherwise low frequent maneuvering simulation. This is a violation of the separation of time scales principle that is underlying to the present method. This issue could still be circumvented in the validation study, which is presented in Section 3.2, by the introduction of dummy propellers that do not exert a force on the ship hull. When the engine response is included, as in Section 4, the wave frequent torque variations will lead to RPM variations that also result in wave frequent thrust variations that affect the low frequent simulation.

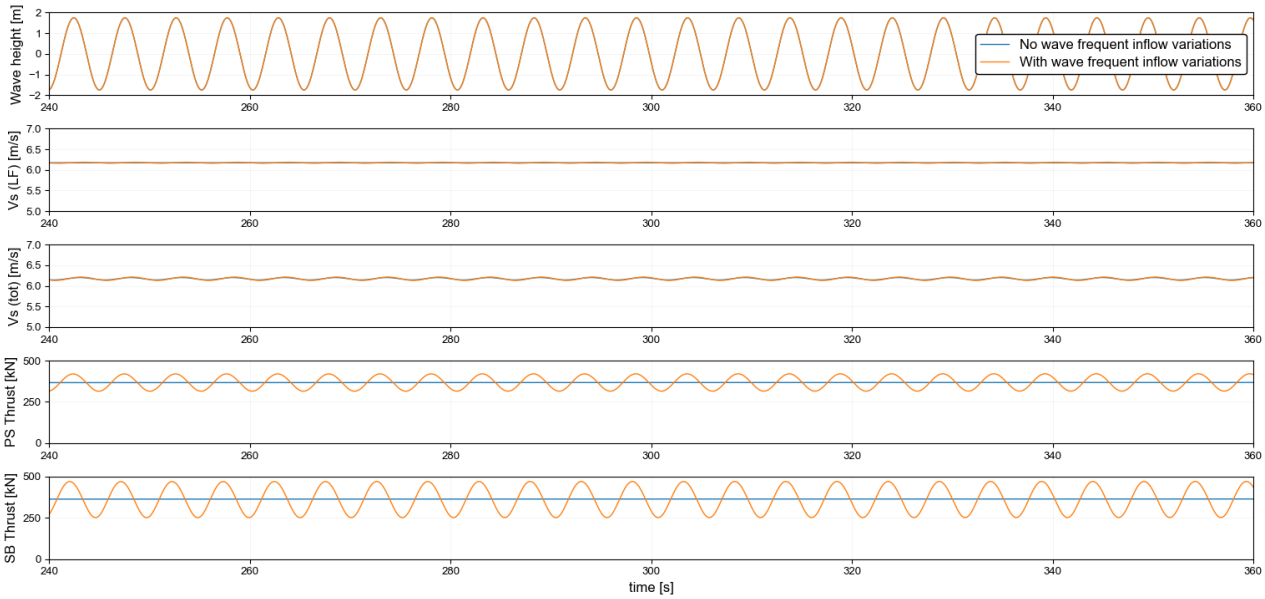

Figure 13: Effect of introducing wave frequent thrust variations in a low frequent simulation. Ship speed of 12 [Kn], bow quartering waves (heading of 135°), wave amplitude of 1.75 [m] and wave frequency of 0.9 [rad/s].

In order to investigate the importance of wave frequent thrust variations Figure 13 shows time traces from two simulations[4]: one in which the wave frequent inflow variations to the propeller were *not* included, and another where they were included. The figure sequentially shows the wave height at the ship's center of gravity, the low frequent (LF) ship speed, the total ship speed (including the wave frequent surge velocity) and the propeller thrust on port and starboard. The effect of the wave frequent inflow variations clearly appears on the propeller thrust signals. There is, however, only a very limited effect on the ship speed, either low frequent and total. Therefore the wave frequent thrust variations do not significantly disturb the separation of time scales principle.

3 VALIDATION OF PROPELLER LOAD VARIATIONS

This section presents a validation study on the load variations on the propellers of the DTMB 5415M combatant, as described by Quadvlieg & Rapuc (2019). The results of simulations are compared with model experiments that were carried out by MARIN for CRS[1]. Table 1 presents the main dimension of the DTMB 5415M hull and propellers.

The model experiments were carried out in MARIN's Seakeeping and Manoeuvring Basin (SMB). During the experiments the model was free sailing. The heading was controlled by an autopilot. The motions of the ship were measured by means of an optical tracking system. The rudder angles and forces were measured, and the propeller thrust and torque were measured. The wave height was measured by various wave probes around the model.

The experiments comprise an extensive program of calm water maneuvering tests (turning circles and zig zag tests for various ship speeds, rudder angles and checking angles) as well as seakeeping tests (heading and track keeping tests in regular and irregular waves for several speeds, headings and wave conditions). This paper presents a limited selection of the results. First the load variations during calm water maneuvers are considered. Then the load variations due to sailing in regular and irregular waves are compared.

All results will be presented at ship scale, but no corrections were applied for the too low Reynolds number at model scale.

Table 1: Main dimensions of DTMB 5415M

Description	Value [unit]
Length between perpendiculars	142.00 [m]
Beam (on water line)	19.09 [m]
Draught (even keel)	6.15 [m]
Displacement	8428.6 [m^3]
Propeller diameter	6.04 [m]
Pitch ratio	0.959 [-]
Expanded area ratio	0.808 [-]
Number of blades	5
Scale ratio (model tests)	30.15

3.1 Propeller Load Variations due to Maneuvering

Figure 14 shows comparisons of simulation results with the model experiments for a 720° turning circle (TC). The charts to the left show results for propellers that are inward rotating over the top. The charts to the right show results for propellers that are outward rotating. Each set of chart shows a bird's eye view of the ship track, and time traces of the rudder angle δ [deg], the ship speed V [Kn],

[4] These are not simulations that are coupled to PPE simulations. The propeller rotation is strictly constant.

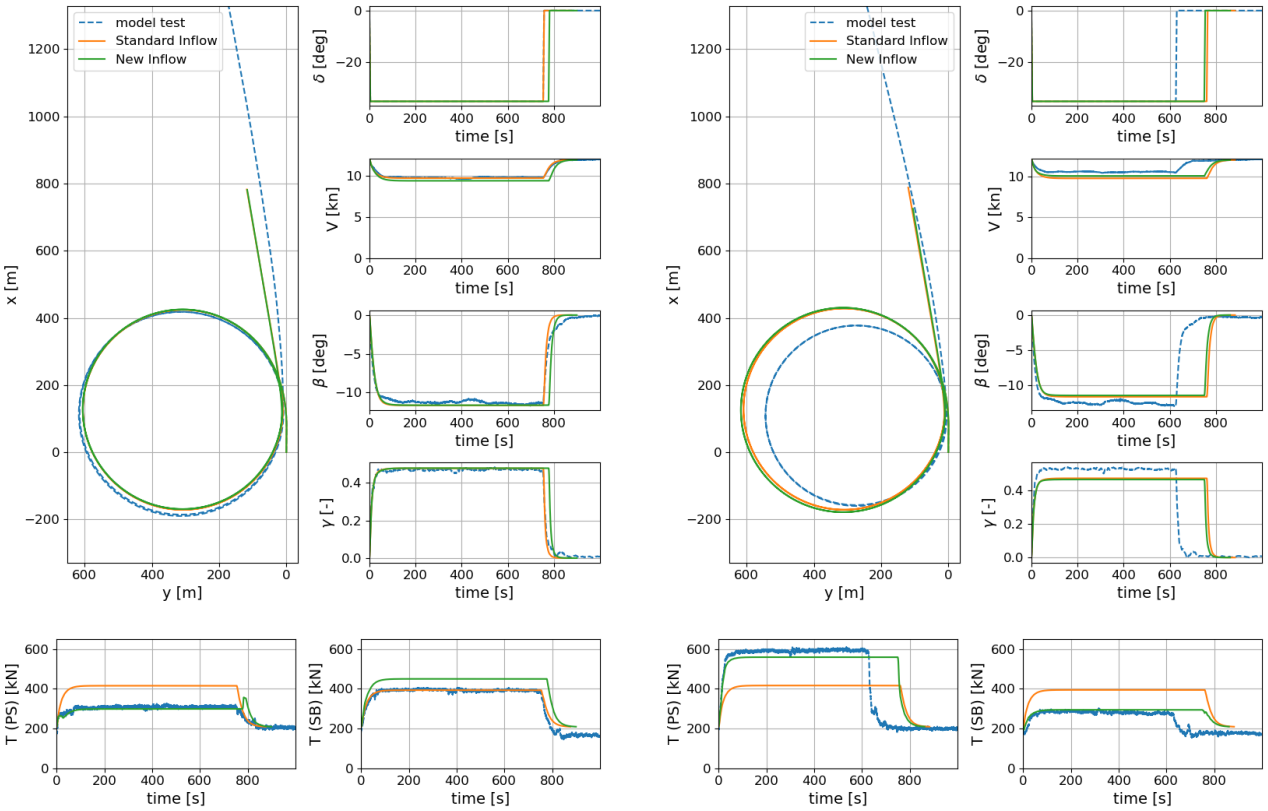

Figure 14: Comparison of simulations with model tests: turning circle to port, approach speed 12 knots, rudder angle 35°. Left: inward rotating propellers. Right outward rotating propellers

the drift angle β [deg], the non-dimensional rotation γ [-][5] and the propeller thrust T [kN] of the port (PS) and starboard (SB) propellers. The torque is not included because it is very similar to the thrust. Each chart shows model experiments, simulation results with the standard inflow model (the undisturbed inflow to the propeller is only multiplied by a constant wake fraction) and the new inflow model that was described in Section 2.2.5.

At time = 0 s, the rudder is actuated while the ship is sailing at a constant approach speed of 12 knots. The rudder quickly moves to a rudder angle of -35°, which is to port. After a few seconds the ship starts turning. The ship speed reduces and the drift angle of the ship increases. During the experiments and the simulations the propeller rotation rate is kept constant at the value that corresponds to the self-propulsion point at the approach speed. The propeller thrust increases due to the lower speed and oblique inflow. After the ship has turned 720° the rudders are rotated back to 0°.

The simulations and experiments are generally in good agreement. The rotation direction of the propellers has a significant effect on the experimental TC diameter, but in the simulations the effect is very limited, irrespective of the inflow model.

The new inflow model does capture some important phenomena that result in a better thrust (and torque) prediction than the standard inflow model. In case of inward rotating propellers (left charts in Figure 14), the port propeller is co-rotating with the vortex that flows into the propeller disk. This results in a strong reduction of the effective RPM and thrust. In case of outward rotating propellers (right charts) the port propeller is rotating against this vortex, which results in a strong increase of the effective RPM and thrust. This effect is, of course, not captured by the standard inflow model. The effect on the starboard propeller, which is on the outside of the turn, is much smaller. Because of this more accurate prediction of the thrust (and torque), the simulation method can also predict the smaller speed loss of the ship with outward rotating propellers.

3.2 Propeller Load Variations due to Waves

The heading keeping in waves experiments were also conducted at a constant propeller rotation rate. The propeller revolutions were, however, increased to overcome the added resistance of the ship due to waves. An autopilot (PID controller) was used to control the heading of the ship. The control parameters in the simulations were the same as in the model tests.

First, the propeller load variations due to sailing in regular waves are presented, then the load variations while sailing in irregular waves are shown.

3.2.1 Regular waves

The wave frequent motions of the ship, that seakeeping code SEACAL predicts, are in good agreement with the experiments for head and bow quartering waves. For stern quartering waves the agreement is less good, in particular

[5] $\gamma = r \cdot L_{pp} / V$, where r [rad/s] is the rotational velocity of the ship about the vertical axis and L_{pp} is the ship's length at perpendiculars

for surge, roll and yaw motions. A comparison of the motions is not included in order to reduce the number of pages of this paper.

There is still an issue with the drift force predictions of SEACAL. On some panels on the sonar dome of the ship, high velocity gradients of the steady (double body) velocity occur, which makes certain contributions to the drift force very large. The determination of the velocity gradients is amongst others discussed by Chen & Malenica (1996) and by Van 't Veer (1998). Their method works fine for motion prediction, but for the drift forces the accuracy is still insufficient. Therefore the velocity gradients were limited to a maximum value, which effectively comes down to a tuning of the added resistance due to waves. This is subject to further research.

Figure 15, Figure 16 and Figure 17 present comparisons of simulation results with the model experiments. They subsequently present the (constant) propeller rotation rate, the mean thrust and the thrust response amplitude operator (RAO) which is the thrust amplitude divided by the wave amplitude. In all figures the subject parameter is plotted as function of the wave encounter frequency. This is the wave frequency as observed from the ship. Table 2 presents the marker and line legend for these figures.

Table 2: Legend for Figure 15 to Figure 17

Symbol	Description
●	Experiment, PS prop, 1.0 [m] wave amplitude
●	Experiment, SB prop, 1.0 [m] wave amplitude
*	Experiment, PS prop, 1.75 [m] wave amplitude
*	Experiment, SB prop, 1.75 [m] wave amplitude
+	Experiment, PS prop, 3.0 [m] wave amplitude
+	Experiment, SB prop, 3.0 [m] wave amplitude
———	Simulation, PS prop, 1.0 [m] wave amplitude
———	Simulation, SB prop, 1.0 [m] wave amplitude
— — — ·	Simulation, PS prop, 1.75 [m] wave amplitude
— — — ·	Simulation, SB prop, 1.75 [m] wave amplitude
·····	Simulation, PS prop, 3.0 [m] wave amplitude
·····	Simulation, SB prop, 3.0 [m] wave amplitude

Thanks to the said tuning of the added resistance, experimental and simulated propeller ration rate (Figure 15) and thrust (Figure 16) are in good agreement. When this tuning is not applied, the simulated propeller revolutions and thrust would be much higher, in particular for encounter frequencies up to 1.2 [rad/s]. The figures show that the propellers must deliver a much higher thrust when the ship sails in high waves, as the drift forces (added resistance) are proportional to the wave height squared. The thrust difference between the port and starboard propellers is caused by the fact that the ship is sailing under a drift angle. In the experiments the difference may also be caused by small propeller geometry differences between the port and starboard propellers.

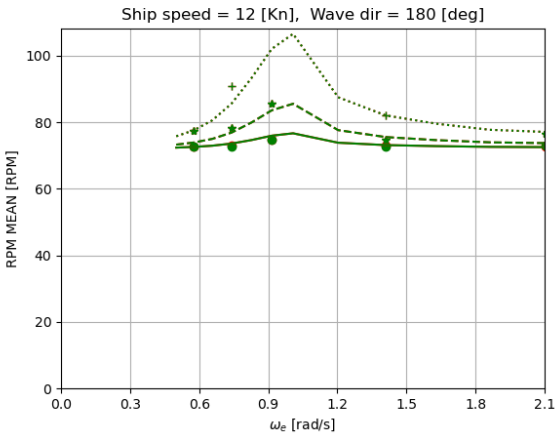

Figure 15: RPM in regular bow quartering waves

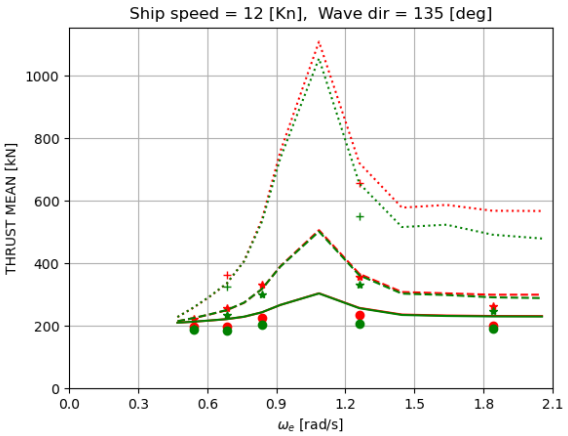

Figure 16: Mean thrust in regular bow quart. waves

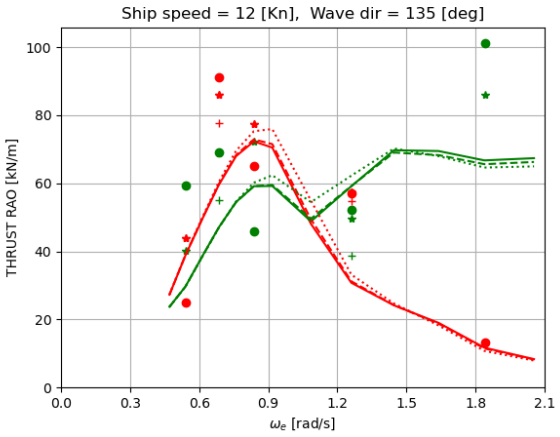

Figure 17: Thrust RAO in regular bow quart. Waves

Figure 17 shows that the experimental and the simulated thrust variations are in reasonable agreement. The simulations do capture the shielding of the leeward (PS) propeller for higher frequencies. The experiments show significant scatter with the wave amplitude. The reason for this is not completely clear. It may be related to non-linear effects or to vortices that are flowing through the propeller disk, like in case of maneuvering.

3.2.2 Irregular waves

Finally, computational and experimental results in irregular waves are compared. Time traces, as shown in Figure 13 and Figure 22, are not very convenient for comparison. First of all, it is hard to ensure that the ship encounters identical waves in the simulation and the experiment. Furthermore, long time traces are required to make a statistically sound comparison. Therefore the comparison is made in terms of statistical properties and as plots of the power spectral density (PSD) of relevant parameters. Again the results for a ship speed of 12 knots and bow quartering waves were selected for presentation in this paper. Furthermore, the sea state in the simulation and the experiment was a significant wave height of 6 [m] and a peak period of 12.4 [s] (sea state 6). A Pierson-Moskowitz wave spectrum was used.

Table 3 presents a comparison of the statistical properties of the simulation and the experiment. The simulation and the experiment are in good agreement.

Table 3: Comparison of statistical properties

	Simulation		Experiment	
Parameter	**Mean**	**Std.**	**Mean**	**Std.**
Surge velocity [Kn]	12.15	0.63	11.81	0.60
Sway velocity [Kn]	0.52	0.63	0.55	0.55
PS propeller rotation [RPM]	78.24	0.00	78.27	1.36
SB propeller rotation [RPM]	78.24	0.00	78.21	1.34
Mean PS thrust [kN]	331.4	87.4	337.2	108.7
Mean SB thrust [kN]	329.1	81.2	299.7	86.8

Figure 18, Figure 19 and Figure 20 subsequently show the PSD plot of the (irregular) waves, surge velocity and thrust. The scaled-up duration of the experiments was slight over half an hour. The duration of the simulation was a full hour. The Welch method and a Hann window with a length of 100 [s] and 50% overlap were used in the determination of the spectra.

Figure 18 plots the wave spectra both as function of the wave frequency with respect to stationary point and as function of the wave encounter frequency. The dotted black line represents the theoretical Pierson-Moskowitz wave spectrum. The solid black line shows the spectrum at a stationary virtual wave probe in the simulation. The dashed blue line represents the spectrum measured by a wave probe on the carriage in front of the model, and the solid blue line represent the spectrum of a virtual wave probe (measuring undisturbed waves) at the ship's center of gravity from the simulation.

Figure 19 shows a comparison of the spectra of the surge velocity from the experiments and the simulations. Both the experiments and the simulations show 2 distinct peaks: one at the peak of the spectrum, and one a much lower frequency which corresponds to the low frequent speed variations of the ship due to the low frequent drift force variations (that are related to wave groups in the irregular seaway). At high frequencies, above 1.1 [rad/s], the surge response of the ship to these short waves is very limited. Therefore the surge velocity PSD is zero while the waves still contain significant energy at these frequencies (blue lines in Figure 18).

Figure 20 shows a comparison of the spectra of the propeller thrust from the experiments and the simulations. These spectra also have the two distinct peaks that are present in Figure 19. The wave frequent thrust variations are underestimated by the simulations, but the low frequent thrust variations are more or less correct. Both simulation and experiment show larger thrust variations for the port propeller at medium frequencies (around 0.8 [rad/s]), while for high frequencies (above 1.2 [rad/s]) the thrust variations are larger on starboard. This is consistent with RAO for propeller thrust that was presented by Figure 17.

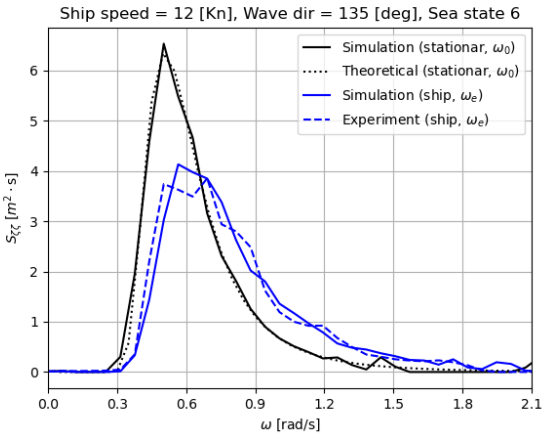

Figure 18: Wave spectrum (PSD)

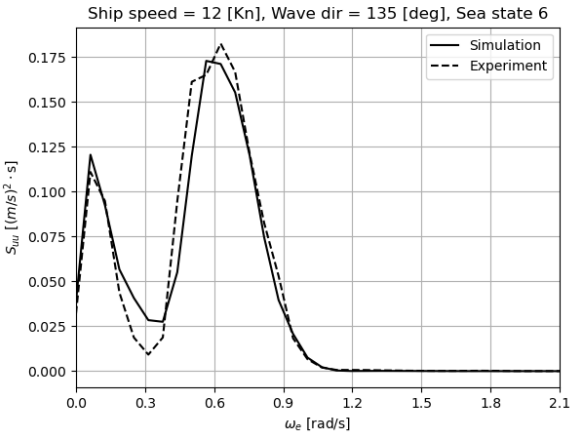

Figure 19: Surge velocity spectrum (PSD)

3.2.3 Other ship speeds and wave conditions

The selected condition of 12 knots and bow quartering waves that was shown in this paper is just one of the wide range of conditions that were tested and simulated. For this condition there is a reasonable agreement between simulations and experiments. It is not the condition for which the correlation is best, but certainly also not the one for which it is worst.

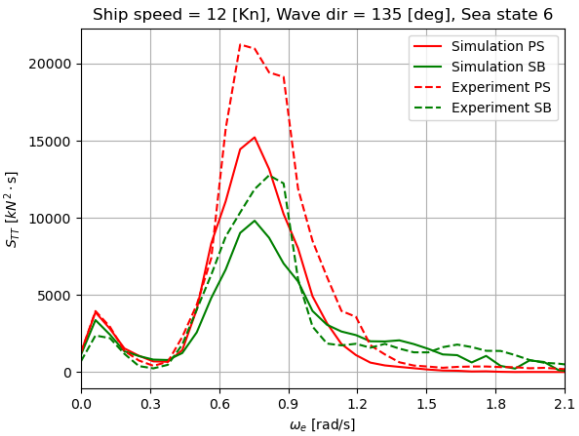

Figure 20: Propeller thrust spectra (PSD)

In general the correlation is reasonable to good for head and bow quartering waves. For stern quartering waves the correlation is less good. At low speed (4 knots) and high waves the heading sometimes cannot be maintained in the simulations while this is still possible in the experiments.

3.2.4 Discussion

The inflow variations of the propeller may be affected by the accuracy of the wave predictions of SEACAL. The effect of the of free surface mesh density and the location of the wave damping zones on the velocities at the propeller disk have never been studied thoroughly. The used (default) values result in accurate predictions of ship motions and added resistance, but not necessarily in accurate velocities at the propellers.

It must be realized that the propeller thrust and torque measurements were not the first point of interest in these experiments. The propellers that were used are rather small, at least much smaller than what MARIN would use in powering tests, and also the accuracy of the propeller geometry is not as high as in powering tests. This model has relatively long propeller shafts which makes the setup susceptible to vibrations. These are not straight forward measurements.

There could be several reasons for the poor correlation in stern quartering waves. The wave encounter frequencies are much lower when the waves come from astern. Then the separation of wave frequent and maneuvering time scales becomes questionable.

The tuning of the drift forces (added resistance) by limiting the velocity gradients of the steady flow works reasonably well for head and bow quartering waves, but for stern quartering waves there is still a large difference.

Furthermore, it seems that the yaw drift forces are also overestimated. This is an important factor for the conditions where the ship cannot maintain it's heading in the simulations. The sway drift forces seem to be more or less correct as the correlation of the drift angle (or the transverse velocity) is in most cases quite good. The sway drift force is also hardly affected by the truncation of the velocity gradients of the steady flow.

Another aspect, that may be relevant for the wave frequent thrust variations in following and SQ waves, is the absence of the rudders in the SEACAL calculations. The rudders could cause a strong diffraction of the incoming waves, which may influence the inflow variations to the propellers. For head and BQ waves the effect of the rudders will be less as they are aft of the propellers.

4 COUPLED SHIP-ENGINE SIMULATIONS

Studies have already shown that dynamics on the propulsion system can affect the Propulsion Power and Energy (PPE) system in terms of fuel consumption, emissions, and power quality of the connected electrical systems (Tavakoli et al 2020, Yum et al 2017, Hou et al 2017, Nasiri et al 2021). For these studies, a coupling between models representing the hydrodynamics and the behavior of the PPE system is essential. Another, benefit of this coupling is that the effect of different control approaches in the engine room can be studied and analyzed during dynamic events.

An example of this is presented in a case-study where two propulsion control approaches, torque control and power control, are compared with a baseline case where the propeller is running at a constant rotational speed. The case study is performed on a simplified PPE model that uses an electrical propulsion system fed by a 1000 V DC-Distribution system. The DC-Bus is connected to two ideal power sources with allowed ramp rates of 10% per second.

Figure 21 shows the PSD of the engine power for the different control strategies. This again concerns the DTMB 5415M sailing at a mean speed of 12 knots in pow quartering irregular waves with a significant wave height of 6.0 m and a peak period of 12.4 s. These results concern the port propeller and engine. The figure clearly shows the difference in the engine power variations for the different control strategies. Constant RPM results in strong wave frequent and low frequent engine power variations, constant torque already strongly reduces the power simulations, while constant power control obviously results in almost zero power variations.

Figure 22 shows time traces of the start of these simulations. Also here the effects of the different control approaches are clearly visible. In torque control mode, there are still significant propeller torque variations. The difference with the constant engine torque results in the rotational acceleration of the drive train. Constant power mode results in reduced power dynamics on the DC-Bus (bottom chart in Figure 22), resulting in an almost constant DC-Bus voltage.

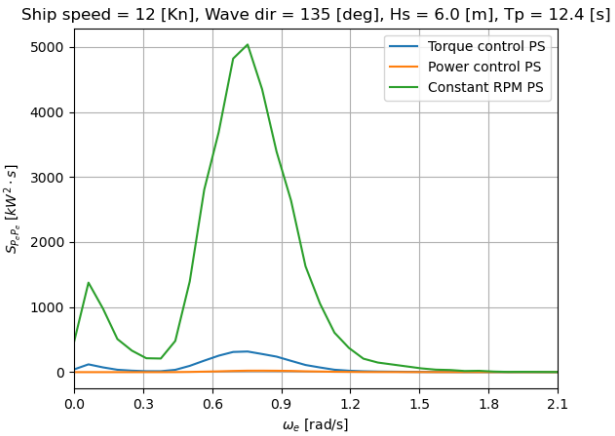

Figure 21: Engine power spectra for different control strategies (PSD)

The simple PPE model was not able to cope with the strong load variations in constant RPM mode. Either the control parameters had to be relaxed, or more capacity had to be added to the DC-grid. Constant torque or constant power seem more attractive from an electrical point of view, but it comes with increased variations in propeller rotation, and therefore also with an increased risk for racing in case of propeller ventilation

The effect of the control strategy on ship speed is only small. There is only a significant effect during the acceleration phase between 0 and 150 s. The effects will become more evident when the operating limits of the PPE system are encountered. This becomes more important when slow reacting power sources or weak grids are included in the PPE system. Therefore, a two-way coupling between the ship hydrodynamics and the PPE system can play a role in early design verification leading to lower risks for new designs.

5 CONCLUSIONS

The mathematical model described in this paper bridges the gap between propulsion, maneuvering and seakeeping. An attempt was made to include all relevant aspects.

The inflow to the propellers when the ship sails under drift or rotation was improved. Next to the axial propeller inflow, the inflow swirl has been introduced. Both depend on the local undisturbed inflow angle at the propeller.

When the ship is sailing in a seaway, the wave frequent inflow variations and the low frequent inflow variations of the propellers are considered. An accurate modeling of the free surface waves around the ship are important for an accurate prediction of the wave frequent load variations. The low frequent load variations follow from maneuvering simulations with an external force that represents the low frequent drift forces.

The simulation method was validated against model experiments with the DTMB 5415M combatant for calm water maneuvers and for sailing in regular and irregular waves.

The improved propeller inflow model results in an important improvement of the propeller thrust and torque predictions during a turning circle. Thanks to the inflow swirl, the simulations also capture the difference in thrust and torque for inward and outward propeller rotation.

For heading keeping in waves, the correlation of thrust and torque variations is reasonably good for head and bow quartering waves. This applies to both the wave frequent and the low frequent variations. For stern quartering waves the correlation is less good.

Finally, the coupling with the (v-)ZEL, brings together the outer (hydrodynamic) and inner (engine room) aspects of the design of a ship in a single workflow. The control strategy of the propeller drive train appears to have a

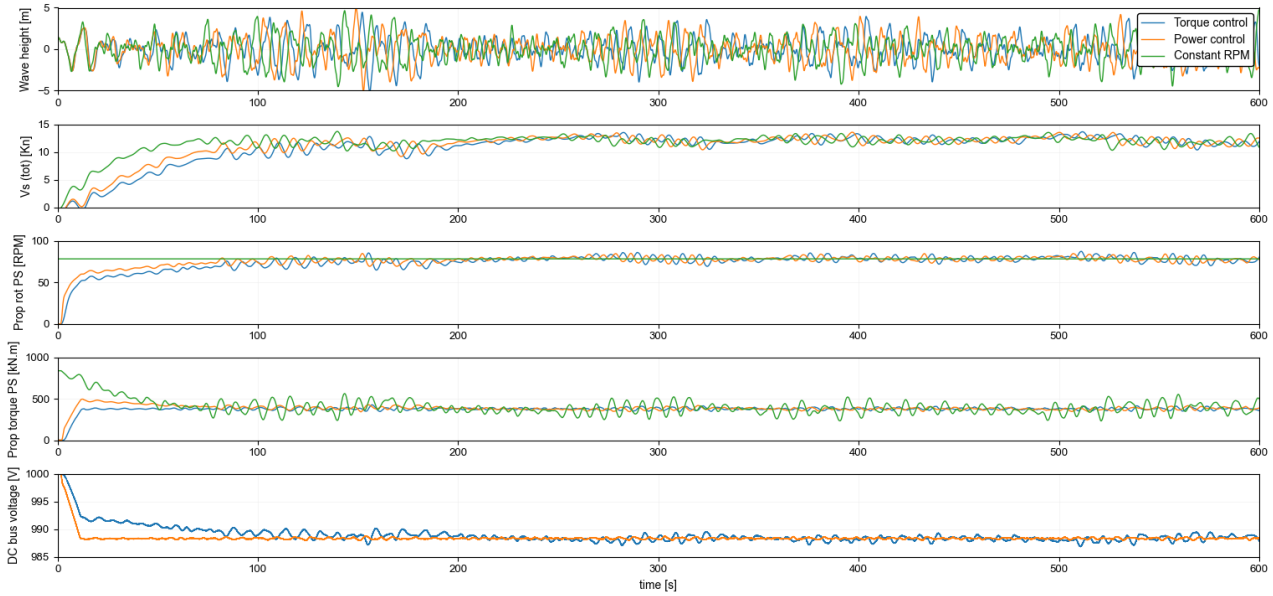

Figure 22: Effect of the control strategy on ship speed, propeller load and DC-bus voltage

strong effect on the load variations that the PPE system experiences.

ACKNOWLEDGEMENT

The CRS, and in particular the CRS SALSA working group, are acknowledged for their support in this research. The following people deserve personal thanks: Tomasz Gornicz (MARIN), Lefteris Kalochristianakis (LR), Adèle Lesage (BV Solutions), Sébastien Loubeyre (BV Solutions) and Davide Grassi (CETENA) for their CFD contributions that led to the new propeller inflow model for ships sailing under drift and/or rotation, as well as Ruddy Kurnia (MARIN) for the preparation of the necessary SEACAL databases.

REFERENCES

Abbing A. (2015), 'XMF leads to development af a multi-purpose simulation platform', MARIN Report, No. 116, December 8, 2015

Bertram V. (1990), A Rankine Source Method for the Forward-Speed Diffraction Problem, PhD Thesis, University of Hamburg, Bericht Nr. 508.

Bunnik T. (1999), Seakeeping calculations for ships, taking into account the non-linear steady waves, PhD thesis, Delft University of Technology, The Netherlands.

Chen X.B. & Malenica S. (1996) 'Uniformly valid solution of the wave-current-body interaction problem', Poceedings 11th International WWWFB, Hamburg.

Ferrari V., Tonelli R., Kisjes A.S. & Hallmann R. (2022), "Manoeuvring experiments, mathematical model and sensitivity analysis for test-case ferry", Martech2022

Hou J., Sun J. & Hofmann H.F. (2017), 'Mitigating Power Fluctuations in Electric Ship Propulsion With Hybrid Energy Storage System: Design and Analysis', IEEE Journal of Ocean Engineering, vol. 43, no. 1, pp. 93-107.

Kuiper G. (1992), The Wageningen Propeller Series, Maritime Research Institute Netherlands (MARIN), Wageningen.

Nakos D.E. (1990), Ship Wave Patterns and Motions by a Three Dimensional Rankine Panel Method, PhD Thesis, Massachusetts Institute of Technology.

Nasiri S., Peyghami S., Parniani M. & Blaabjerg F. (2021), 'Modeling in-and-out-of-water impact on all-electric ship power system considering propeller submergence in waves', IEEE Transportation Electrification Conference & Expo (ITEC), Chicago.

Quadvlieg F. H. H. A. & Rapuc S. (2019), 'A pragmatic method to simulate maneuvering in waves', SNAME Maritime Convention, Tacoma, WA.

Rijpkema D., Starke B. & Bosschers J. (2013), 'Numerical simulation of propeller-hull interaction and determination of the effective wake field using a hybrid RANS-BEM approach', Third International Symposium on Marine Propulsors smp'13, Launceston, Tasmania, Australia.

Tavakoli S., Saettone S., Steen S., Andersen P., Schramm J. & Pedersen E. (2020), 'Modeling and analysis of performance and emissions of marine lean-burn natural gas engine propulsion in waves', Applied Energy, vol. 279.

Van 't Veer (1998), Behaviour of catamarans in waves, PhD thesis, Delft University of Technology, The Netherlands.

Vaz, G. (2005), Modelling of sheet cavitation on hydrofoils and marine propellers using boundary element methods, PhD Thesis, Instituto Superior Técnico, Lisbon, Portugal, 2005.

Vaz, G. & Bosschers, J. (2006), 'Modelling of three dimensional sheet cavitation on marine propellers using a boundary element method', 6th Int. Symp. on Cavitation CAV2006, Wageningen, The Netherlands

Yum K., Taskar B., Pedersen E. & Steen S. (2017), 'Simulation of a two-stroke diesel engine for propulsion in waves', International Journal of Naval Architecture and Ocean Engineering, vol. 9, pp. 351-372.

Yasukawa H, & Nakayama Y. (2009), '6-DOF motion simulations of a turning ship in regular waves', MARSIM International Conference on Marine Simulation and Ship Manoeuvrability, pages 508–517, Panama City, Panama.